01 Oct 2013

Making Reliable Shear-Wave Splitting Measurements

Kelly H. Liu
Missouri University of Science and Technology, liukh@mst.edu

Stephen S. Gao
Missouri University of Science and Technology, sgao@mst.edu

Making Reliable Shear-Wave Splitting Measurements

by Kelly H. Liu and Stephen S. Gao

Abstract   Shear-wave splitting (SWS) analysis using *SKS*, *SKKS*, and *PKS* (hereafter collectively called *XKS*) phases is one of the most commonly used techniques in structural seismology. In spite of the apparent simplicity in performing SWS measurements, large discrepancies in published SWS parameters (fast direction and splitting time) suggest that a significant portion of splitting parameters has been incorrectly determined. Here, based on the popularly used minimization of transverse energy technique, we present a procedure that combines automatic data processing and careful manual screening, which includes adjusting the *XKS* window used for splitting analysis, modifying band-pass filtering corner frequencies, and verifying and (if necessary) changing the quality ranking of the measurements. Using real and synthetic data, we discuss causes and diagnostics of a number of common problems in performing SWS analysis, and suggest possible remedies. Those problems include noise in the *XKS* window being mistaken as signal, non-*XKS* seismic arrivals in the *XKS* window, excessive use of null ranking, measurements from misoriented sensors and from sensors with mechanical problems, and inappropriate dismissal of usable measurements.

Introduction

Several decades of geophysical studies concluded that anisotropy is a nearly ubiquitous property of the Earth's crust and mantle. Among the many techniques capable of investigating such anisotropy, splitting of *P*-to-*S* converted phases from the core–mantle boundary (CMB), among which the most commonly used ones are *SKS*, *SKKS*, and *PKS* (which are collectively called *XKS*), provides the best lateral resolution due to the steep angle of incidence of the *XKS* arrivals. Because they are *P*-to-*S* converted phases from the CMB, the *XKS* phases are radially polarized at the CMB; consequently, when the original north–south and east–west components are rotated to the radial and transverse components, any *XKS* energy on the transverse component indicates the existence of azimuthal anisotropy from the CMB to the recording station (Silver, 1996). On the other hand, the absence of transverse energy, which is termed as a null measurement, does not always indicate the absence of anisotropy. This is because when the back azimuth of the *XKS* event is close to the fast or slow direction, the *XKS* phase barely splits, leading to unobservable energy on the transverse component. Relative to direct *S* waves, which are arbitrarily polarized, the known polarization direction of the *XKS* phases at the CMB leads to reliable determination of the splitting parameters (the polarization direction of the fast wave and the splitting time between the fast and slow waves). As demonstrated by numerous previous studies (Vinnik *et al.*, 1989; Silver and Chan, 1991; Silver, 1996; Savage, 1999; Long and Silver, 2009), along with seismic tomography and receiver function stacking, shear-wave splitting (SWS) analysis has become a

routinely utilized technique in structural seismology. Consequently, splitting parameters have been measured at the vast majority of broadband (sometimes short-period, e.g., Gao *et al.*, 1994) three-component seismic stations on Earth, frequently by multiple research groups.

Unfortunately, due to various reasons (some of which are discussed in this paper), very large discrepancies for the same stations are sometimes found among results reported by different studies (e.g., Liu *et al.*, 2008, for station BJT). One of the causes for such discrepancies is the different measuring techniques used to conduct the measurements. As discussed in Vecsey *et al.* (2008), among the three most commonly used techniques, including minimization of energy on the transverse component, minimization of eigenvalue of the covariance matrix, and maximization of cross-correlation between the resulting fast and slow components (Ando, 1984; Silver and Chan, 1991; Savage and Silver, 1993), the minimization of transverse energy technique is the most stable one when noise is present. Not surprisingly, it is arguably the most commonly used technique among all the SWS measurement techniques. The minimization of transverse energy technique grid searches for the optimal pair of splitting parameters that most effectively remove the energy on the transverse component (Fig. 1). For quality control purposes, once the optimal parameters are found, the fast and slow components, which should have similar waveforms if the resulting parameters are reliable, are computed by rotating and time shifting the original radial and transverse components (Fig. 1).

LSAxxx_IC (29.700, 91.150); BAZ=112.82°, Dist=89.75°
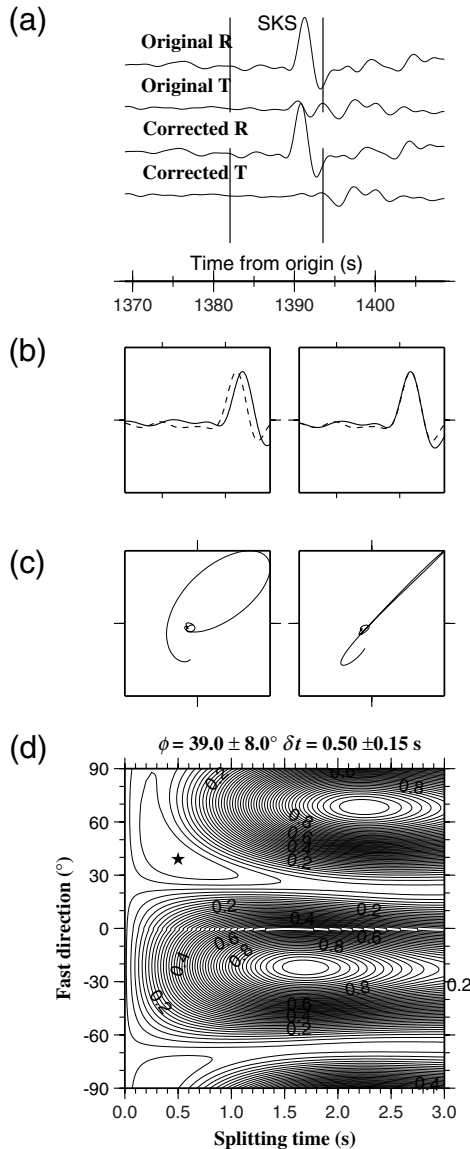
EQ992612351; Ev-lat=-19.71; Ev-long=169.21;
Ev-Dep=103km

(a)

Original R
SKS

Original T

Corrected R

Corrected T

Time from origin (s)
1370 1380 1390 1400

(b)

(c)

(d)

$\phi = 39.0 \pm 8.0°$ $\delta t = 0.50 \pm 0.15$ s

Fast direction (°)

Splitting time (s)

Figure 1. Diagrams associated with an SWS measurement at station LSA. (a) Original radial, original transverse, corrected radial, and corrected transverse components. The section between the two vertical bars is the *XKS* window used for SWS analysis. Note that for this event–station pair, there is a non-*XKS* arrival immediately following the right boundary of the *SKS* window. Unconstrained splitting parameters were obtained when the non-*XKS* arrival was included in the splitting analysis. Shown on top are station and event names and locations. Note that station names in the figures have six characters (and for those with less than six characters, the name is padded by x's) and are followed by the network code. (b) The left plot shows resulting fast (dashed) and slow (solid) components, and in the right plot the slow component is advanced by the optimal splitting time. (c) Particle motion patterns for the original fast and slow (left plot) and shifted fast and slow (right plot) components shown in (b). (d) Contour of energy on the corrected transverse component as a function of trial fast directions and splitting times. The star indicates the optimal splitting parameters corresponding to the minimum energy.

Another possible cause of the discrepancies is the presence of complex anisotropy and spatial variations of anisotropic properties beneath a station. Virtually all the existing measurement techniques assume simple anisotropy (i.e., a single layer of anisotropy with a horizontal axis of symmetry, which hereafter is called a "horizontal layer" for simplicity, although a layer with a horizontal axis of symmetry is certainly not necessarily horizontal) beneath a station. The term complex anisotropy refers to forms of anisotropy other than simple anisotropy, and for most cases of complex anisotropy, the observed splitting parameters vary as a function of the back azimuth of the seismic events. The observed splitting parameters for complex anisotropy are thus apparent splitting parameters.

To improve the reliability of SWS measurements, several studies (Savage, 1999; Teanby *et al.*, 2004; Vecsey *et al.*, 2008; Wustefeld *et al.*, 2008) provide brief but valuable suggestions on the "best practices" in data preprocessing, splitting parameter measurements, and results ranking. In addition, recently we proposed a semiautomatic procedure for reliably and rapidly measuring and objectively ranking SWS parameters (Liu *et al.*, 2008; Gao and Liu, 2009; Liu, 2009; Gao *et al.*, 2010) in response to the dramatic increase of broadband seismic data such as those recorded by the ongoing USArray project (Liu, 2009; Refayee *et al.*, 2013). However, at the present time there still is not a systematic treatment of the various potential problems in SWS measurements that caused the discrepancies. Here, aided by numerous synthetic and real data examples, we present a detailed description of the procedure, discuss some common problems that partially contributed to the discrepancies among previous studies, and suggest possible remedies. While we understand that not everyone in the SWS community uses the procedure or the Silver and Chan (1991) method that the procedure is built upon, it is clear to us that most of the standards and problems presented below are common to other SWS measurement techniques.

A Procedure for Making Reliable SWS Measurements

Requesting Data

The cutoff magnitude used by most previous studies is in the range of 5.7–6.0, and the epicentral distance range is 84°–140°. To ensure that data from all potentially useful events are requested from the Incorporated Research Institutions for Seismology (IRIS) Data Management Center (DMC), our procedure uses a lower cutoff magnitude of 5.6, which is reduced to 5.5 if the focal depth is greater than 100 km to take the advantage of sharper waveforms from deeper earthquakes. Data from events with magnitudes at or above the cutoff magnitude and in the epicentral distance range of 84°–180° are requested from the IRIS DMC. The requested traces start from 100 s before the theoretical arrival time of the first compressional wave and are 1100 s long. Because the useful

epicentral distance ranges for *SKS*, *PKS*, and *SKKS* are 84°–180°, 120°–180°, and 90°–180°, respectively, the epicentral distance range (84°–180°) used for requesting data is sufficiently wide to include all three phases. In other words, a single trace may contain all three different phases in different time windows, and thus there is no need to request data separately for each of the three phases. Note that while in principle *SKKS* arrives ahead of *S* wave at a distance greater than 85.3° for surface events, only those with distance ≥90° are used to ensure sufficient separation between *SKS* and *SKKS*, which are usually used together to generate a single pair of splitting parameters in the distance range of 84°–90°.

Data Selection

The original files requested from the DMC are converted into Seismic Analysis Codes (SAC) format, resampled into a uniform sampling rate of 20 samples per second, and sorted into event directories. The SAC files are then detrended and band-pass filtered in the frequency band of 0.04–0.5 Hz, which includes the main *XKS* energy, and the horizontal north–south (N–S) and east–west (E–W) components are rotated to radial and transverse components. The initial *XKS* window is selected as the section between $a = T_{XKS} - 5.0$ s and $f = T_{XKS} + 20$ s, where T_{XKS} is the theoretical arrival time of the *XKS* phase calculated using the IASP91 earth model. Note that the *XKS* window starts 5 s before the theoretical *XKS* arrival time to avoid exclusion of the beginning of the *XKS* wavetrain when errors in the determination of the origin time and/or the focal location are large. The extra pre-*XKS* time section is also used for easy identification of non-*XKS* arrivals as well as for visually judging the noise level during the manual screen stage. If direct *S* or S_{diff} arrives in the *XKS* window, f is reset as 5 s before the theoretical arrival time of direct *S* or S_{diff}. As discussed below, the initial corner frequencies and the start and end times of the *XKS* window are subject to manual adjustment during the visual screening stage.

An automatic trace selection procedure is then applied to reject event–station pairs with low signal-to-noise ratio (SNR) on the radial component. The pair is rejected if SNR < 4.0; SNR is defined as $\max |A_{(a,f)}|/\text{mean}|A_{(a-10,a)}|$, in which $\max |A_{(a,f)}|$ is the maximum absolute value on the original radial seismogram in the *XKS* time window between a and f, and mean$|A_{(a-10,a)}|$ is the mean absolute value on the seismogram in the time window between $a - 10$ s and a. The automatic event selection procedure typically rejects about 60% of the *SKS* and 70% of the *PKS* and *SKKS* event–station pairs obtained from the DMC. The rejected seismograms are visually verified to ensure that no traces with visible *XKS* arrivals are excluded from further process.

Automatic SWS Measurement and Result Ranking

A procedure based on the minimization of transverse energy criterion is then applied to the selected traces to obtain the splitting parameters (Liu *et al.*, 2008). Auto-ranking of resulting SWS measurements is performed using a combination of SNR on the original radial, original transverse, and corrected transverse components. Quality A and B measurements have outstanding and good (respectively) *XKS* arrivals on both the original radial and transverse components, and near perfect removal of *XKS* energy on the corrected transverse component; null measurements (Quality N) have outstanding *XKS* arrivals on the original radial component but no *XKS* arrivals on the original transverse component; and Quality C measurements have weak *XKS* arrivals on the original radial component. For events with strong *XKS* arrivals on both the original radial and transverse components, but in which the *XKS* energy cannot be effectively removed on the corrected transverse components, a Quality of S (for "special") is given. The cutoff SNR values for each of the ranking categories are shown in figure 5 of Liu *et al.* (2008).

Manual Screening

Manual screening is aimed at correcting misdeterminations of the automatic measuring and ranking procedure, by adjusting the start and end of the *XKS* window, filtering parameters, and quality ranking.

Adjusting the Start and End of the XKS *Window.* This is perhaps the most important step to ensure reliable SWS measurements. The purposes of the adjustment are excluding non-*XKS* arrivals and reducing the standard deviation (SD) of the measurements. The Silver and Chan (1991) procedure estimates the SD using the inverse *F*-test, by assuming that the energy on the corrected transverse component has a χ^2 distribution. In general, small SDs can be obtained if the window includes only the most robust portion of the *XKS* arrival and when the SNR is high. The original Silver and Chan SWS code assigns an SD of 22.5° for the fast direction when the measurement is totally unconstrained. The reason for assigning this particular value for unconstrained measurement is that at the 95% confidence interval, which approximately corresponds to two standard deviations, the possible values of the fast direction cover a 90° range (±45°) and are thus unconstrained. Therefore, the maximum SD is set as 22.5°. If there is convincing *XKS* signal on both the original radial and transverse components, considerable efforts should be made to adjust the a and/or f values several times (and possibly the filtering parameters; see Adjusting Filtering Parameters) to bring the SD of the fast direction to a value smaller than 22.5°.

Because non-*XKS* arrivals usually cannot be effectively removed by the optimal splitting parameters, the onset of non-*XKS* arrivals can be identified from the corrected transverse components. Once the onset is identified, the a and more frequently the f value of the *XKS* window can be manually adjusted to exclude the non-*XKS* arrivals. The new window should lead to reduced SDs for both the fast direction and the splitting time. The example shown in Figure 1 is from station LSA on the Tibetan Plateau (Gao and Liu,

2009). When the original *XKS* window is used (which extends to 10 s to the right of the window shown in Fig. 1), the resulting parameters are $45 \pm 22.5°$ and 0.50 ± 2.23 s, which are totally unconstrained. A careful examination of the corrected transverse component finds an uncorrected signal that follows the peak of the *SKS* phase by about 5 s (Fig. 1). Moving the right boundary of the *XKS* window to the point just ahead of the non-*XKS* arrival led to well-defined splitting parameters of $39 \pm 8°$ and 0.50 ± 0.15 s.

Adjusting Filtering Parameters. Some *XKS* arrivals are contaminated by strong noise or non-*XKS* seismic arrivals with frequency contents that are significantly different from those of the *XKS* signal (Fig. 2). In order to obtain correct splitting parameters and to reduce the SDs, one or both of the cutoff frequencies used for band-pass filtering should be adjusted (Fig. 3). Sometimes it is necessary to experiment with different combinations of the frequencies to find the one that leads to the most reliable measurements, which are indicated by the small SDs and reasonable match between the resulting fast and slow waveforms.

Manually Altering Quality Ranking. Quality ranking is performed quantitatively based on the combination of SNR on the original radial, original transverse, and corrected transverse components (Liu *et al.*, 2008). As demonstrated by the example shown in Figure 4, Quality A measurements have all of the following features, including (1) outstanding *XKS* arrivals on both the original radial and transverse components, (2) the resulting optimal splitting parameters effectively removed almost all the *XKS* energy on the corrected transverse component, (3) the original particle motion pattern is elliptical, and the corrected particle motion pattern is linear or close to linear, and (4) there is a well-defined minimum on the contour map of energy on the corrected transverse component, and consequently the SDs for both the fast direction and the splitting time are small (e.g., less than 10° for fast direction, and less than 0.5 s for splitting time). Quality B measurements (Fig. 5) have slightly lowered quality measures relative to Quality A measurements. Both Quality A and B measurements are used in the interpretation of the results. Quality C measurements are not used for interpretation. They usually result from weak (relative to the noise) *XKS* arrivals on the original radial and/or transverse component. As a result, the similarity between the resulting fast and slow waveforms is low; so is the linearity of the corrected particle motion pattern. In addition, the contour plot lacks a well-defined minimum, and the SDs are usually large. While the presence of any of the above can be used to justify a Quality C measurement, the most important considerations are the lack of strong *XKS* energy on the original transverse component and the lack of similarity between the fast and slow waveforms.

The N (or null) ranking (Fig. 6) should only be given to those with outstanding SNR on the radial component but with confirmed lack of *XKS* energy on the original transverse

PFOxxx_II(33.610, -116.460), BAZ= 305.82°, Dist=91.94°
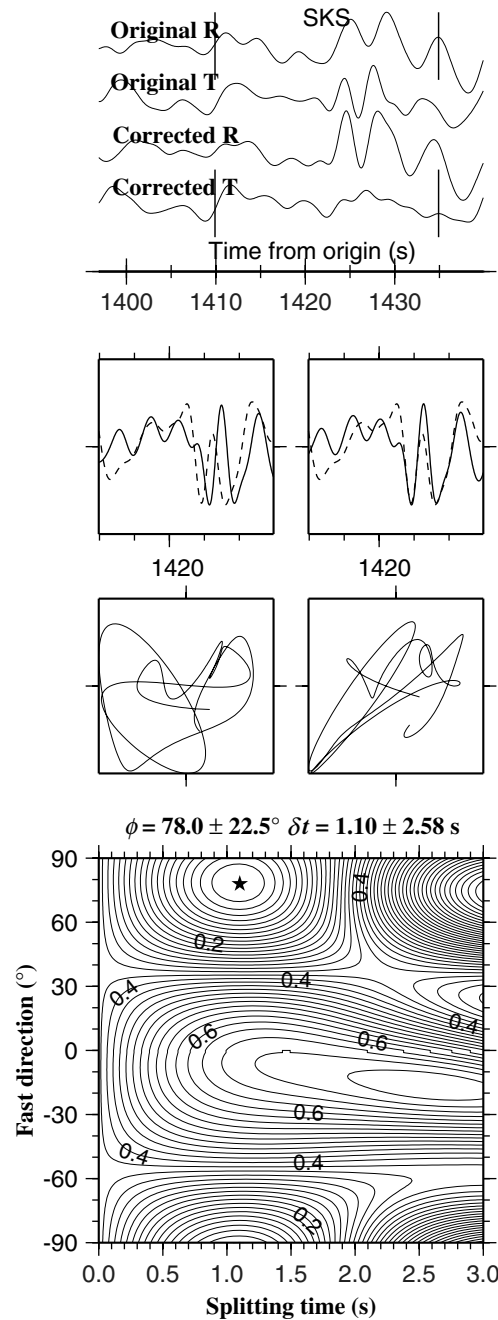EQ952920032; Ev-lat=28.16, Ev-long=130.16; Ev-Dep=33km

Figure 2. Same as Figure 1, but for seismograms contaminated by low frequency noises. The seismograms were filtered using the initial corner frequencies of 0.04–0.5 Hz.

component. Note that there is a fundamental difference between Quality N measurements and Quality C measurements, and many automatically ranked Quality N measurements should be manually changed to Quality C. Because Quality C events are not manually verified, due to their huge quantity (except for a visual checking of the measured results without going through the waveforms), the automatic

PFOxxx_II(33.610, -116.460), BAZ= 305.82°, Dist=91.94°
EQ952920032; Ev-lat=28.16, Ev-long=130.160; Ev-Dep=33km

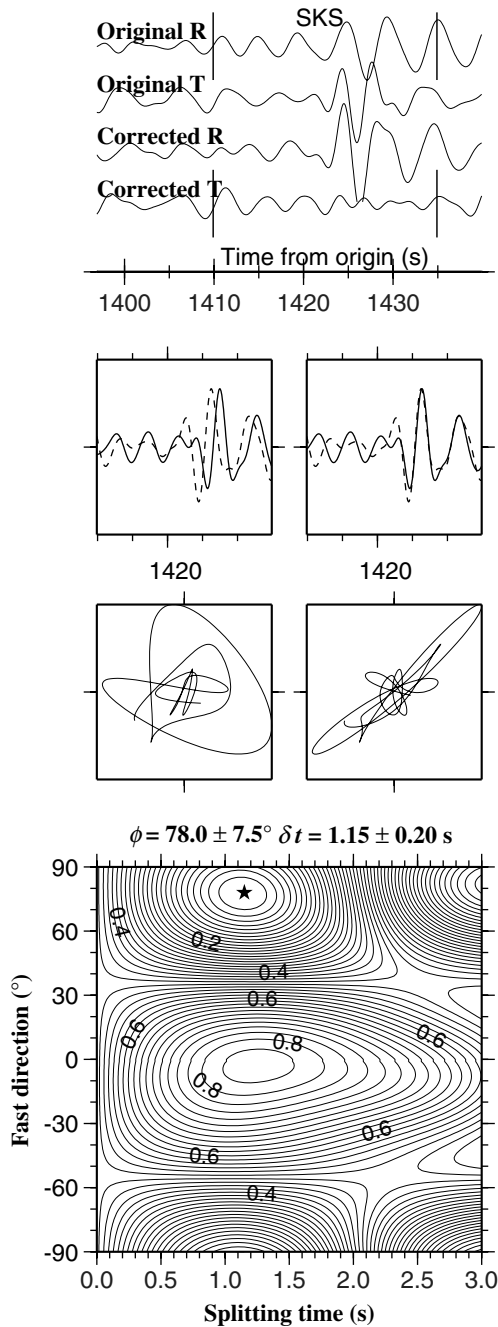$\phi = 78.0 \pm 7.5° \ \delta t = 1.15 \pm 0.20$ s

Figure 3. Same as Figure 2 but after the corner frequencies are adjusted from 0.04–0.5 Hz to 0.15–0.5 Hz. Note the significant improvement of the SNR, similarity between the resulting fast and slow components, and linearity of the corrected particle motion pattern.

ranking procedure intentionally sets low SNR thresholds on the original radial and transverse components for Quality N measurements to minimize the possibility of missing good measurements. The common problem of excessively assigning Quality N measurements is discussed in a later section.
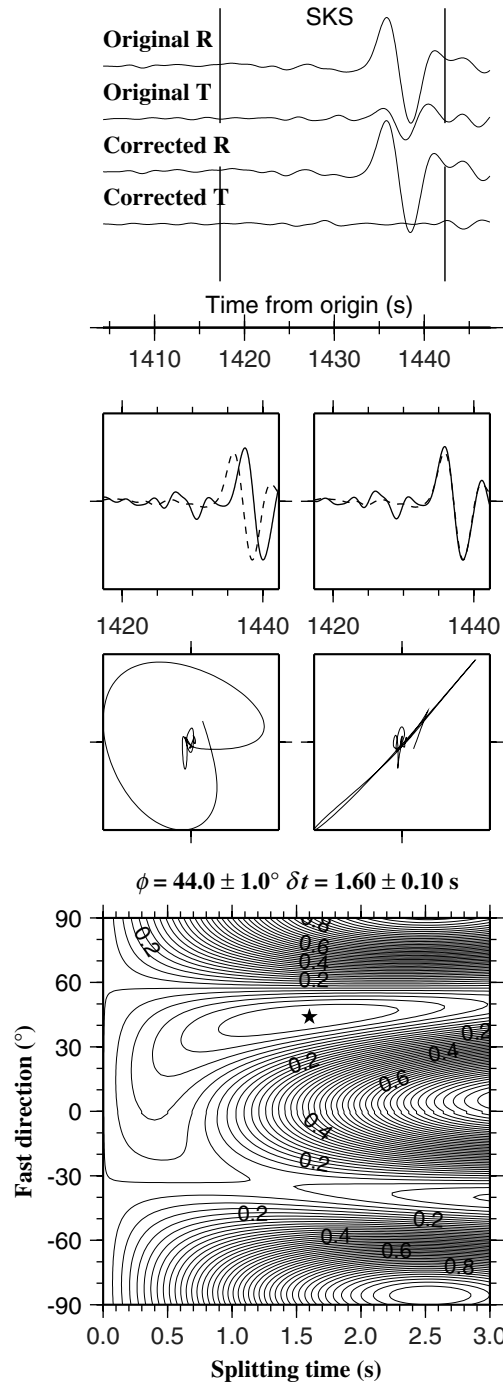
FURIxx_IU(8.900,38.680); BAZ=57.42°, Dist=95.40°
EQ973142306; Ev-lat=31.19;Ev-long=140.49; Ev-Dep=86km

$\phi = 44.0 \pm 1.0° \ \delta t = 1.60 \pm 0.10$ s

Figure 4. Example Quality A measurement.

Identification of Complex Anisotropy

Identification of complex anisotropy at the measurement stage not only paves the road for reasonable interpretation of the SWS results but is also critical for understanding the waveforms and particle motion patterns. A quick realization of the existence of complex anisotropy at a station is also important

FURIxx_IU (8.900, 38.680); Baz=63.36°, Dist=97.98°
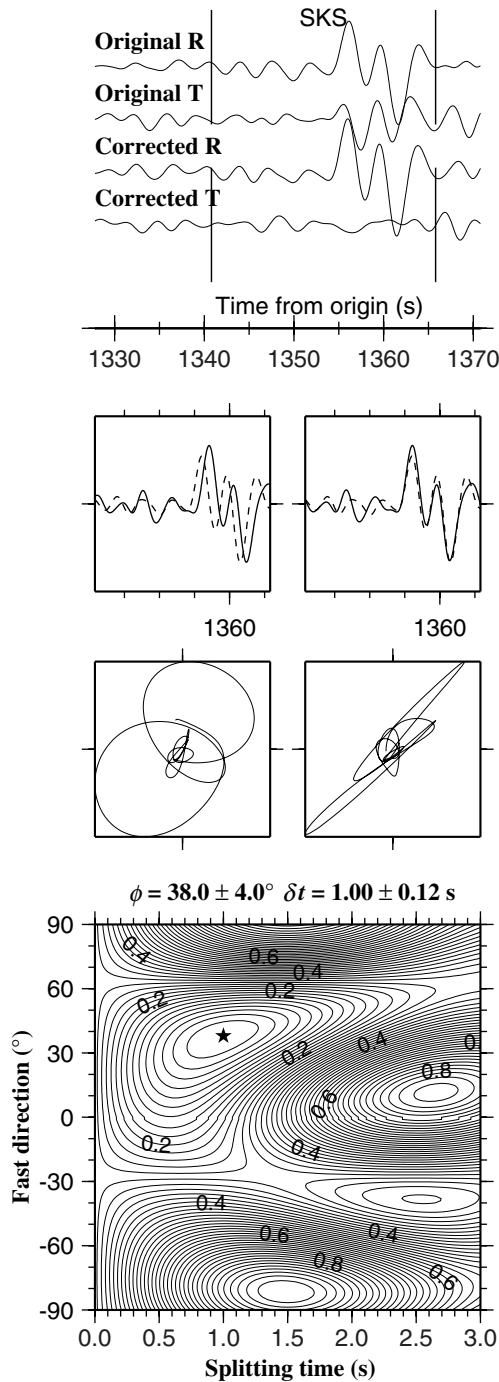**EQ980380118; Ev-lat=24.82; Ev-long=141.75;Ev-Dep=525km**

$\phi = 38.0 \pm 4.0°$ $\delta t = 1.00 \pm 0.12$ s

Figure 5. Example Quality B measurement.

USINxx_NM (37.970, -87.670), BAZ=319.25°,Dist=128.21°
EQ050361223; Ev-lat=5.29, Ev-long=123.34; Ev-Dep=525km

$\phi = 56.0 \pm 22.5°$ $\delta t = 0.40 \pm 2.17$ s

Figure 6. Example Quality N measurement.

for manual adjustment of quality ranking. For instance, as described below, because complex anisotropy frequently results in incomplete removal of *XKS* energy on the corrected transverse component, a quality ranking of "S" (for special measurements with significant remaining energy on the corrected transverse component) could be given by the automatic rank-
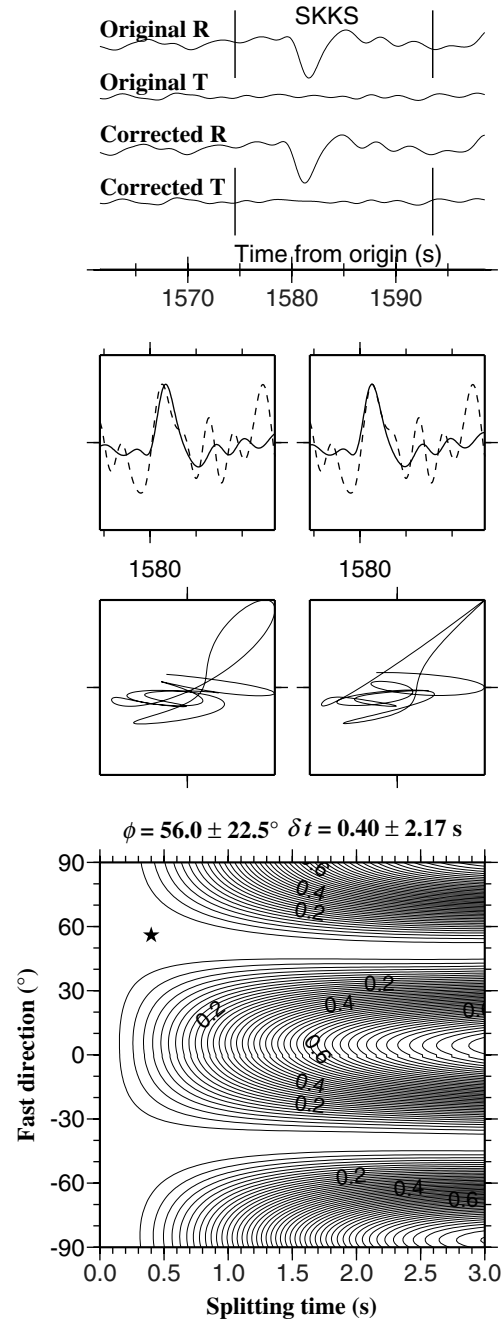
ing procedure, and the measurement is abandoned (because only A and B measurements are used for interpretation). However, if the operator realizes that remaining *XKS* energy on the transverse component is a normal feature for complex anisotropy, as demonstrated by the synthetic test below, the ranking of such measurements should be changed to A or B.

Simple Versus Complex Anisotropy. From the point of view of SWS measurements, simple anisotropy also refers to the

cases when two or more horizontal layers have identical or orthogonal fast directions. When two or more horizontal layers have the same fast direction, the resulting fast direction is the same as the fast direction of all the layers, and the measured splitting time Δt is the sum of that of the individual layers, that is, $\Delta t = \sum_{i=1}^{n} \delta t_i$, in which n is the number of layers and δt_i is the splitting time of the ith layer. Similarly, for multiple layers in which n_1 layers have a fast direction of ϕ and n_2 layers have a fast direction of $\phi + 90°$, the splitting time of the system is the absolute value of the difference between the combined splitting time of each of the two groups, i.e., $\Delta t = |\Delta t_1 - \Delta t_2|$, in which $\Delta t_1 = \sum_{i=1}^{n_1} \delta t_i$ is the combined splitting time for layers in group 1, and $\Delta t_2 = \sum_{i=1}^{n_2} \delta t_i$ is the combined splitting time for layers in group 2. The fast direction is ϕ if $\Delta t_1 > \Delta t_2$, and is $\phi + 90°$ if $\Delta t_2 > \Delta t_1$. Obviously, the special situation of $\Delta t_1 = \Delta t_2$ leads to an apparent isotropic medium and overwhelmingly null measurements.

Simple anisotropy is hinted by the existence of null measurements from events with a back azimuth that is parallel or orthogonal to the fast direction obtained from non-null measurements at the station, and by near-perfect removal of *XKS* energy on the corrected transverse component. For simple anisotropy, none of the resulting fast-direction measurements should exist along the lines defined by $\phi = A$ and $\phi = A + 90°$, in which ϕ is the observed fast direction and A is the modulo-90° back azimuth (Fig. 7).

The most common forms of complex anisotropy that can be reasonably constrained by SWS analysis include two horizontal layers (Silver and Savage, 1994) and a single layer with a dipping axis of symmetry (Levin *et al.*, 2007). The former is characterized by systematic azimuthal variations of the apparent parameters with a 90° periodicity (Fig. 8), and the latter by a 180° periodicity. For a given station, if the azimuthal coverage of the events used for SWS measurement is reasonably good, the existence of complex anisotropy can easily be judged by the presence of systematic azimuthal variations of the measured splitting parameters.

When the azimuthal coverage is poor, other diagnostics should be used to identify the existence of complex anisotropy. For most forms of complex anisotropy, pure null measurements can hardly be observed. For instance, in a two-horizontal-layer model, each of the two layers has nonzero splitting time, and the fast directions are not parallel or orthogonal to each other. The shear wave traveling through the area with such a two-layer structure splits twice: the fast and slow wave produced by the lower layer split again after traveling through the top layer, resulting in four arrivals that cannot be visually observed due to the much smaller splitting times relative to the period of the *XKS* waveform (Silver and Savage, 1994; Menke and Levin, 2003).

Synthetic Tests. To better understand the effects of complex anisotropy on SWS analysis and on ranking of the results, we generate synthetic seismograms from a two-layer model composed by a lower layer with $\phi_1 = 50°$ and $\delta t_1 = 1.0$ s
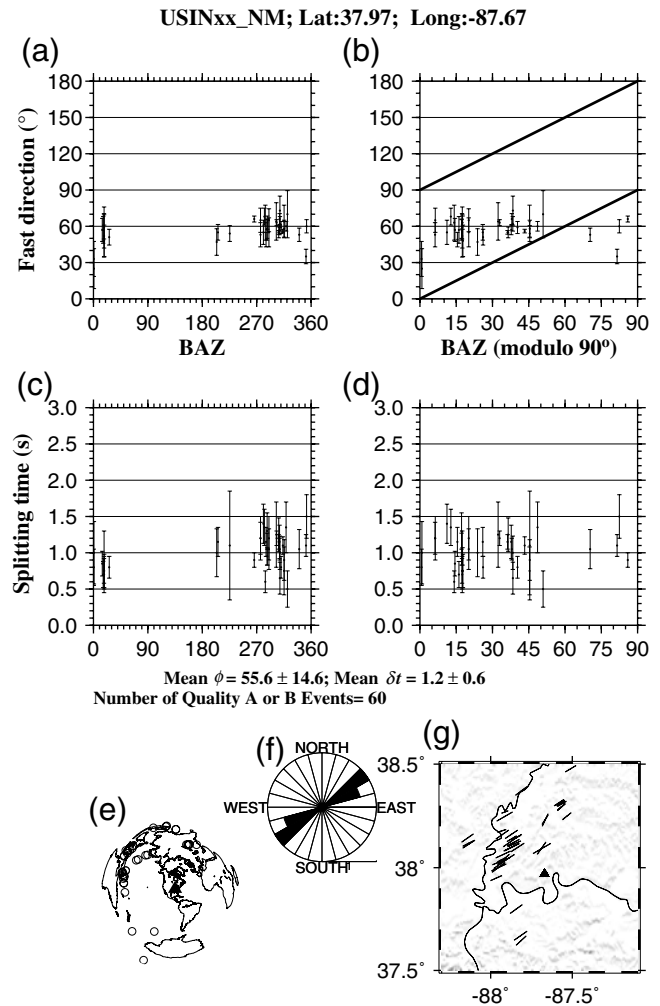

Figure 7. Splitting parameters measured at station USIN in the vicinity of the New Madrid Seismic Zone. (a) Fast directions plotted against back azimuth. (b) Fast directions plotted against modulo-90° back azimuth. The two gray lines have a slope of 45° and indicate where null measurements are expected for simple anisotropy. (c) Splitting times plotted against back azimuth. (d) Splitting times plotted against modulo-90° back azimuth. (e) An azimuthal equidistant projection map showing distribution of *XKS* events used to produce the measurements. The triangle at the center of the map indicates the station. (f) Rose diagram showing distribution of fast directions. (g) Splitting parameters plotted above ray-piercing points at 200 km deep.

and an upper layer with $\phi_2 = 20°$ and $\delta t_2 = 0.6$ s. The presplitting shear wave has the form of $R(t) = A_0 \sin(2\pi f t)e^{-\alpha t}$, in which $A_0 = 100.0$ is the amplitude, $f = 0.15$ Hz is the frequency, and $\alpha = 0.1$ is the decay factor. The original radial and transverse components are computed for 90 events with back azimuths ranging from 0° to 89° and an interval of 1°. The original transverse components are shown in Figure 9a. Apparent SWS parameters are then measured using the synthetic seismograms (Fig. 9d,e).

The synthetic test suggests that there is always energy on the original transverse component (i.e., pure null measurements are nonexistent) although the transverse energy is merely a few percent of that of the presplitting shear wave
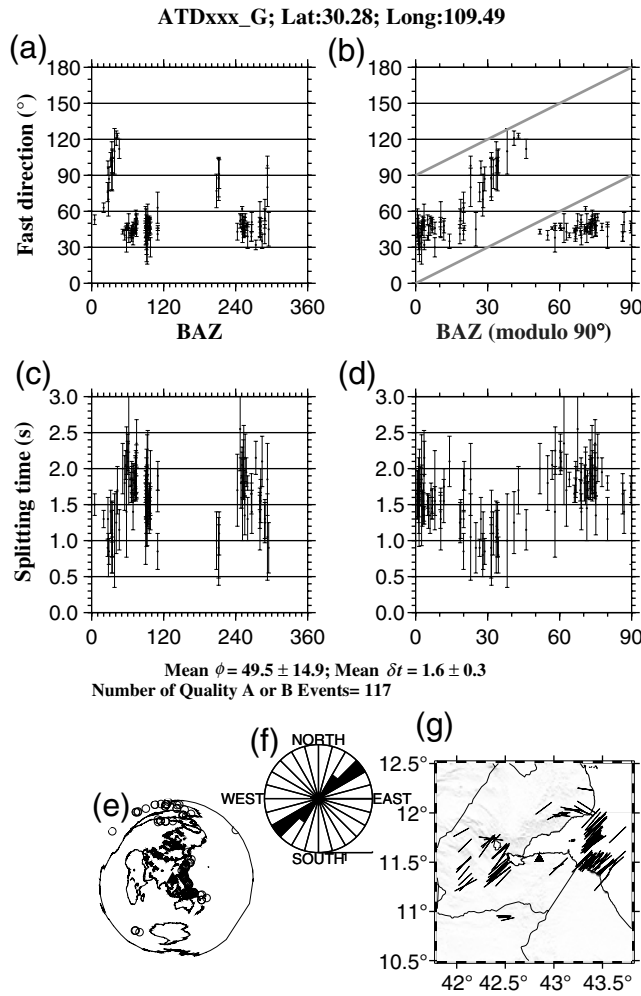
ATDxxx_G; Lat:30.28; Long:109.49

Figure 8. Azimuthal variations of splitting parameters observed at station ATD in the Afar Depression, Ethiopia. Systematic azimuthal variations with a 90° periodicity suggests a two-layer structure beneath the station (Gao *et al.*, 2010).

in the BAZ range of 35°–45° (Fig. 9b). It also indicates that *XKS* energy on the corrected transverse component cannot be totally removed, except for the special case when the back azimuth is equal to the fast direction of the lower layer (Fig. 9c). This is because the minimization of transverse energy technique (and most other techniques) assumes simple anisotropy and also assumes that the *XKS* ray path arrives at the layer of anisotropy along the great-circle arc. When the back azimuth is the same as (or at a right angle to) the fast direction of the lower layer (i.e., when BAZ = ϕ_1, which is 50° for the specific model shown in Fig. 9), the *XKS* ray does not split while traveling through the lower layer, and the resulting apparent parameters are identical to those obtained from a simple anisotropy model with only the top layer. Obviously, at this special back azimuth (hereafter we call it θ_0), the apparent splitting parameters reflect those of the upper layer.

It is well known that the grid search of the two pairs of splitting parameters under a two-layer model using apparent splitting parameters suffers from serious nonuniqueness
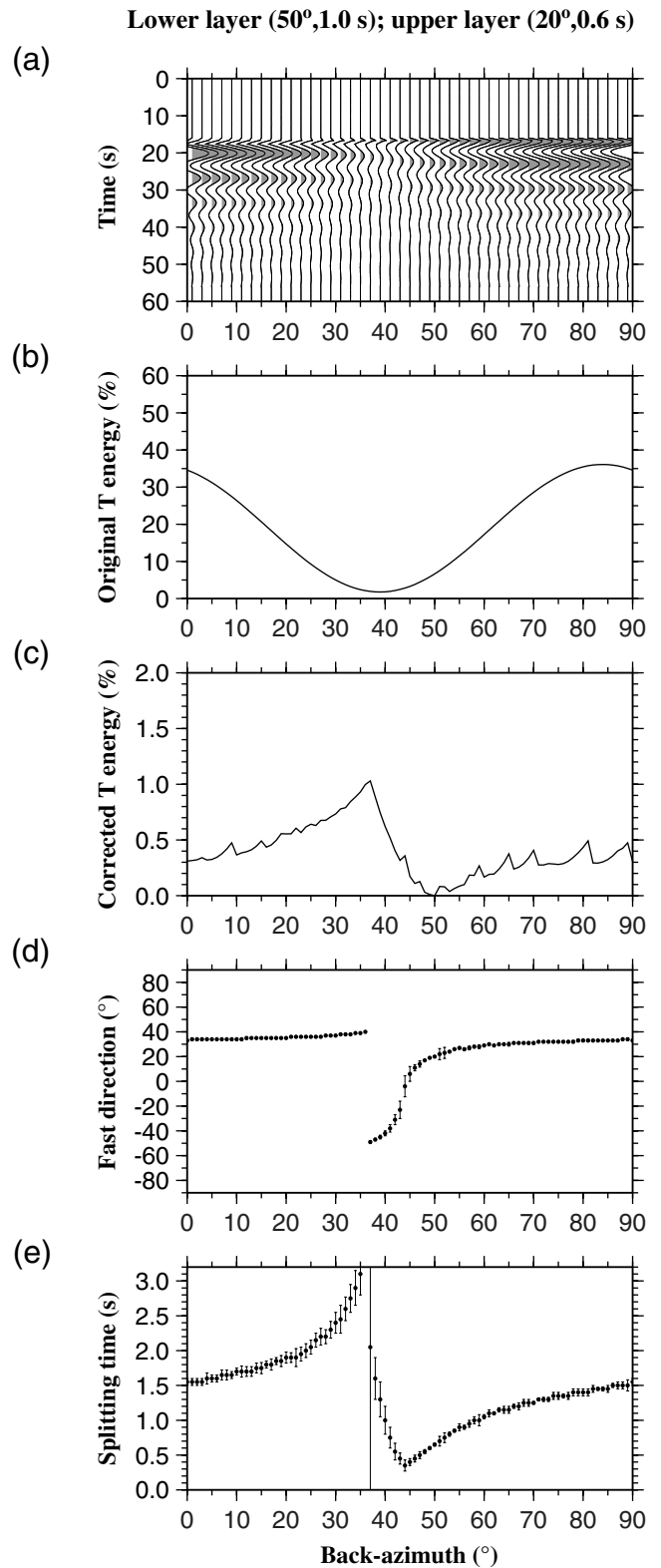
Lower layer (50°,1.0 s); upper layer (20°,0.6 s)

Figure 9. Results of synthetic tests using a two-layer model. (a) Original transverse components (note that only the even number traces are shown for clarity). (b) Energy on the original transverse components displayed as a percentage of that of the presplitting shear wave. (c) Same as (b) but for the corrected transverse components. (d) Resulting apparent fast directions. (e) Resulting apparent splitting times.

problems, due to the trade-offs among the four parameters (e.g., Gao and Liu, 2009). The nonuniqueness can be reduced using the observations from the synthetic test (Fig. 9). First of all, the fast direction of the lower layer is simply θ_0, at which energy on the corrected transverse component is the lowest. Second, as discussed above, the fast direction and splitting time of the upper layer are identical to the apparent splitting parameters corresponding to θ_0, because *XKS* rays with this special back azimuth do not split (Fig. 9d,e). Third, the remaining parameter (i.e., the splitting time of the lower layer) can then be found using a grid search. The four-parameter grid search becomes a one-parameter grid, and consequently the nonuniqueness as well as the computing time reduce dramatically. Of course, the above procedure requires a decent azimuthal coverage (in the modulo-90° domain) by high-quality *XKS* events.

Spatially Varying Simple Anisotropy. A special type of complex anisotropy is spatially varying simple anisotropy (i.e., the fast direction and/or splitting time is different for different ray paths, due to the fact that the station is located near the boundary of two or more regions of simple anisotropy with different splitting parameters). This results in splitting parameters that vary as functions of ray-piercing locations. An excellent example of this type of complex anisotropy is found at station ENH, a station located in the city of Enshi, Hubei Province, China. Events from the north have northwest–southeast fast directions, while those from the southeast result in mostly northeast–southwest fast directions (Fig. 10). This type of complex anisotropy implies that the source of the anisotropy is deeper than the intercept depth of the first Fresnel zones (Alsina and Snieder, 1995; Liu and Gao, 2011).

Some Common Problems in Conducting SWS Measurements

In this section we discuss some of the most common problems based on our own experience. Most of them are also found in previous studies.

Noise in the *XKS* Window is Mistaken as Signal

Nonseismic noise of various origin can often be mistaken as legitimate *XKS* arrivals and sometimes can result in reasonably matched fast and slow components and a well-defined minimum on the contour plot. The most effective way to distinguish between *XKS* signal and noise is to look beyond the *XKS* window. If arrivals with similar characteristics (shape, duration, amplitude, and frequency composition of waveform) also exist outside the *XKS* window, the measurement should be dismissed by changing the quality ranking to C.

In addition to the above approach, another useful practice to exclude measurements from signal-mimicking noise is to compare the resulting splitting parameters with those from
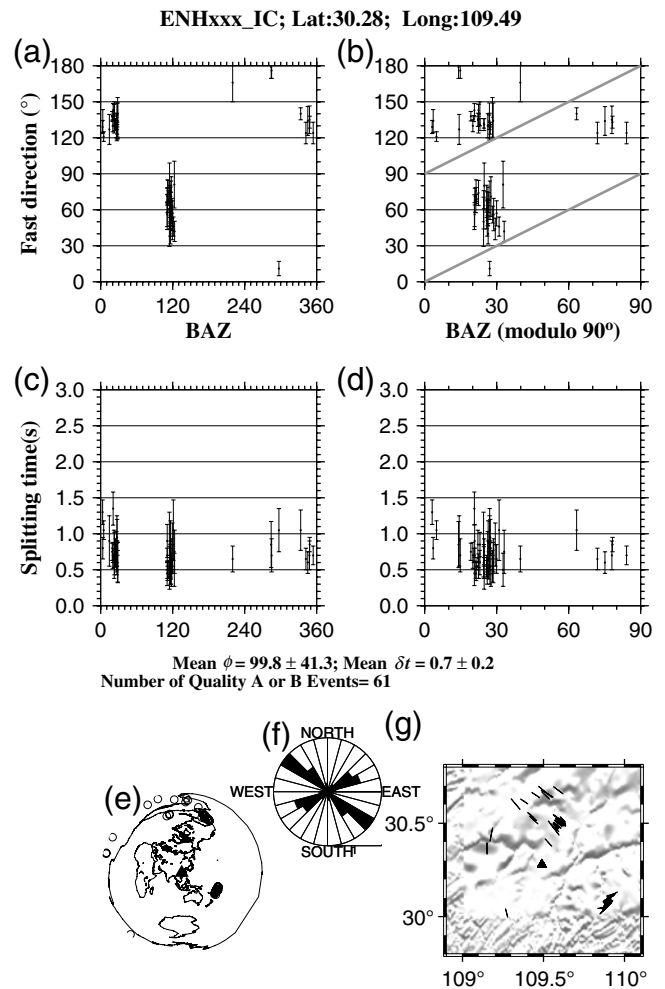

Figure 10. Splitting parameters measured at station ENH in southern China, showing strong dependence of the fast directions on the location of ray-piercing points.

events with outstanding SNR. Significant differences in the parameters usually indicate that the measurement from the noise is erroneous.

Non-*XKS* Seismic Arrivals in the *XKS* Window

Under certain combinations of the epicentral distances and origin times between the *XKS* event of interest and other events, non-*XKS* arrivals from other events can coincidentally arrive at approximately the same time as the *XKS* phase originating from the *XKS* event, leading to erroneous splitting parameters. The seemingly strong *SKS* arrival at station PFO in California shown in Figure 11 is actually the horizontal component of the *P* wave from an M_w 6.6 focal depth = 119.6 km event in South America that occurred about 910 s after the *SKS* event (M_w 5.9, focal depth 88.3 km) in Papua New Guinea. The epicentral distance is 92.54° for the latter and 47.35° for the former. The *SKS* wave from the first event arrives at the station about 5 s earlier than the direct *P* wave from the second event and is totally obscured by the strong *P* wave (Fig. 12).

PFOxxx_II(33.610, -116.460),BAZ=265.77°,Dist=92.53°
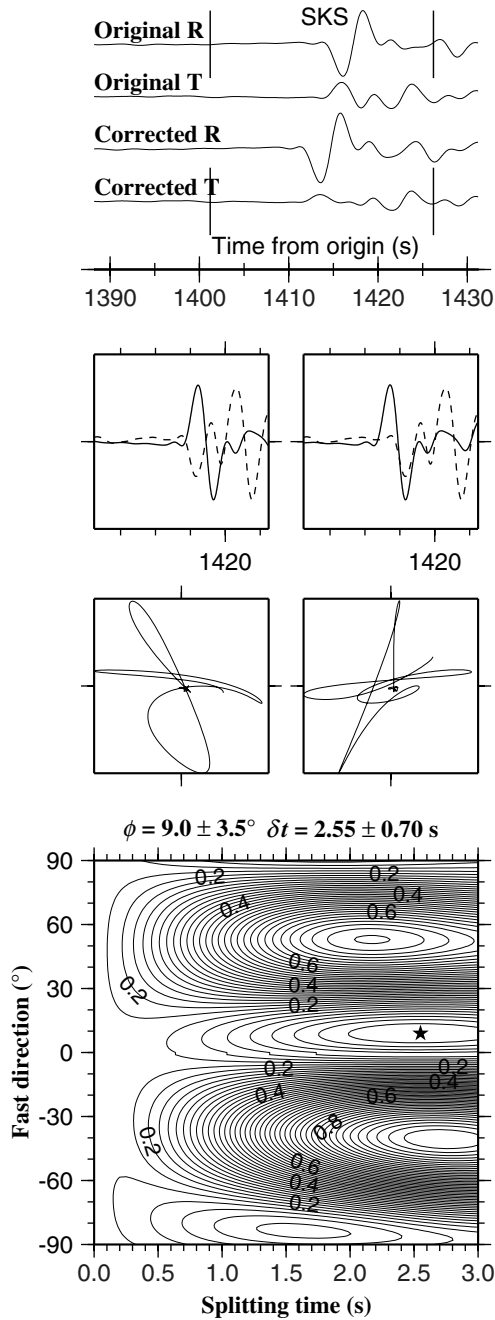**EQ952312128; Ev-lat=-4.96, Ev-long=153.76; Ev-Dep=88km**

Figure 11. Apparently strong *SKS* arrivals but poorly defined splitting parameters, caused by the *P* wave from another event arriving at approximately the same time as the *SKS* wave (see Fig. 12 for locations of the *P* and *SKS* events).

The most common non-*XKS* seismic arrival is the direct *S* wave from the same *XKS* event in the *SKS* window for events with epicentral distance of 85° or smaller. For such events, the *SKS* is followed by the *S* wave by less than 6 s. Care must be taken to move the right boundary of the *XKS* window sufficiently toward the left to exclude the *S* wave.
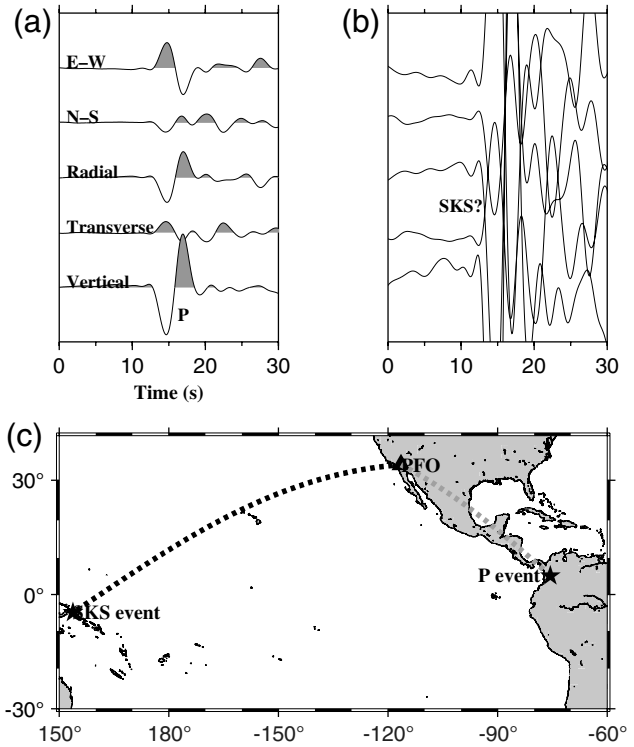

Figure 12. (a) *P* and *SKS* seismograms recorded by station PFO from the two events shown in (c). The strongest arrival is the *P* wave from the event on South America. (b) Same as (a) but the vertical scale is exaggerated by 10 times in an attempt to visually observe the *SKS* phase, which arrived at the station about 5 s before the *P* wave. (c) A map showing station (triangle) and event (stars) locations and the *P* and *SKS* ray paths.

One or more of the following observations can be used to identify non-*XKS* arrivals in the *XKS* window. First, checking the relative amplitude of the vertical component in the *XKS* window. For a true *SKS* or *SKKS* arrival, the amplitude on the vertical component should be much smaller than that on the original radial component. On the contrary, if the arrival is an *S* wave from a local or regional event, or a *P* wave (Fig. 12), the amplitude on the vertical component should be comparable to or even greater than that on the horizontal component. Note that this diagnostic does not work for *PKS*, because *SKP* arrives at the same time at the station as *PKS* and shows up with large amplitude on the vertical component. Second, for non-*XKS* waves, usually the energy on the corrected transverse component cannot be effectively removed. Third, the resulting fast and slow components have a low similarity, and the splitting parameters may have large uncertainties and are not consistent with results from other events. Obviously, measurements from non-*XKS* arrivals should be abandoned.

Excessive Use of Null Ranking

Strictly speaking, the null (or N) ranking should only be given to events with absolutely no energy on the original transverse component. As discussed in Gao and Liu (2009),

ULNxxx_IU(47.865,107.053); BAZ=117.22°, Dist=95.84°
EQ962400624; Ev-lat=-22.57;Ev-long=-179.79; Ev-Dep=575km

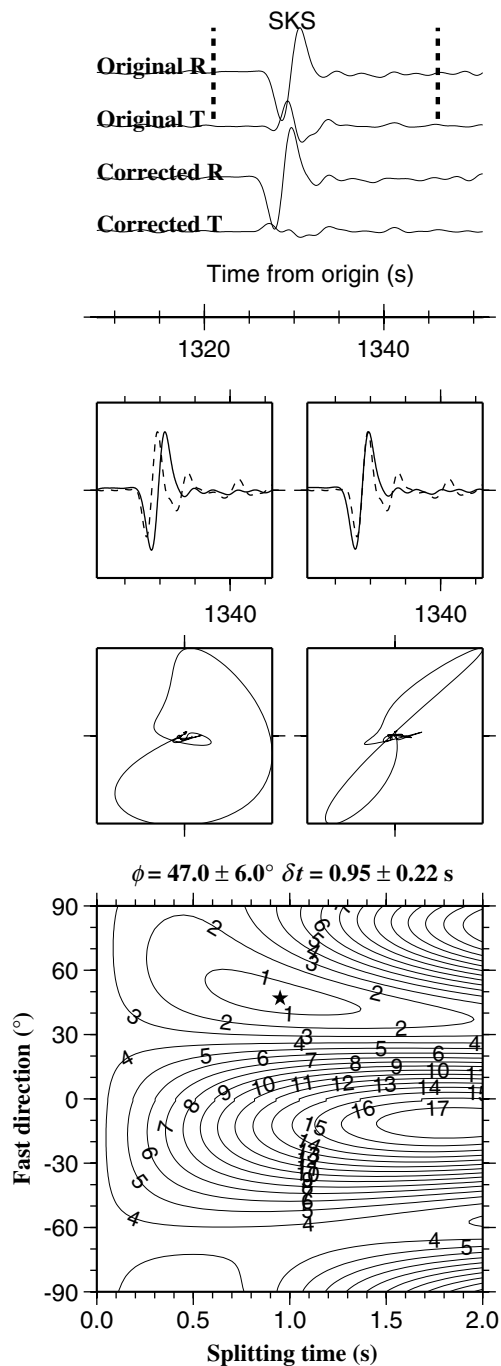$\phi = 47.0 \pm 6.0°$ $\delta t = 0.95 \pm 0.22$ s

Figure 13. Diagrams related to SWS analysis from an event recorded by station ULN in central Mongolia using the minimization of transverse energy technique. Note the poor linearity of the corrected particle motion pattern due to sensor misalignment (Liu *et al.*, 2008).

theoretically such an ideal situation does not exist, due to factors such as finite source size, scattering, off-great-circle arrivals, and departure from a perfect single layer of anisotropy with horizontal axis of symmetry. Therefore,

for a transverse seismogram with noise (which always exists for realistic data), many previous studies inappropriately assigned a null ranking when the *XKS* signal is actually present on the original transverse component but is obscured by the noise. The null (or, more correctly, near-null) ranking should only be given to events with very strong *XKS* arrivals on the radial component and very weak energy on the transverse component in the *XKS* window (Fig. 6). Clearly, this is a subjective criterion. Sometimes no *XKS* arrivals can be observed on the original transverse component, but the splitting analysis led to well-matched fast and slow components. This suggests that there is still significant energy on the original transverse component, and consequently the measurement should not be given a null ranking. Wustefeld and Bokelmann (2007) proposed a criterion for identifying null measurements.

Measurements from Misoriented Sensors

The minimization of transverse energy technique assumes that the seismograms were recorded by seismometers with the north–south component pointing exactly to the geographic north pole. The actual orientation of the horizontal sensors might be significantly different from this ideal situation, due to errors made when the stations were installed. For instance, a recent study shows that about 10% of the early EarthScope Transportable Array stations were misoriented by 5° or more (Ekstrom and Busby, 2008).

As discussed in Liu *et al.* (2008) using data from station ULN and by Tian *et al.* (2011) using synthetic data, one of the diagnostics of sensor misorientation is that the *XKS* energy on the transverse component cannot be effectively removed by the optimal splitting parameters when the minimization of transverse energy approach is used, and the final particle motion pattern is not linear (Fig. 13). In this case, the minimization of eigenvalue technique, which simultaneously searches for the arriving azimuth of the *XKS* phase, more effectively removes transverse energy and yields a more linear particle motion (Fig. 14; Liu *et al.*, 2008). To obtain the correct parameters, the horizontal seismograms should be rotated prior to splitting analysis, so that the corrected north–south component points to the geographic north. The amount of rotation can be obtained by searching for the angle that gives the most-linear particle motion. The minimization of transverse energy approach and the minimization of eigenvalue approach should result in similar splitting parameters from correctly rotated data.

Measurements Using Data Recorded by Malfunctioning Instruments

One of the most common forms of instrumental malfunctioning is that one of the two horizontal sensors inside a seismometer stopped working, producing a false seismogram with constant (normally all zero after data detrending) amplitudes. Failure to unlock, serious sensor tilting, and breakdown of the electronics are among the most

ULNxxx_IU(47.865,107.053); BAZ=117.22°, Dist=95.84°
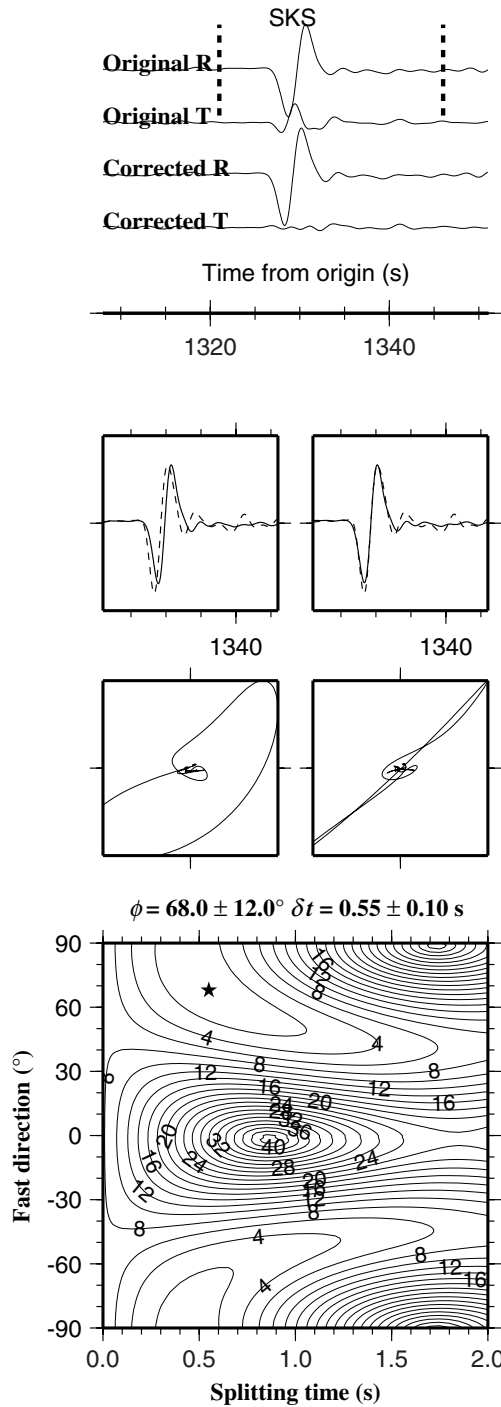**EQ962400624; Ev-lat=-22.57;Ev-lon=-179.79; Ev-Dep=575km**

USINxx_NM(37.970, -87.670), BAZ=323.61°, Dist=91.00°
EQ112040434; Ev-lat=38.90, Ev-long=141.82; Ev-Dep=41km

$\phi = 68.0 \pm 12.0°$ $\delta t = 0.55 \pm 0.10$ s

$\phi = -18.0 \pm 2.5°$ $\delta t = 3.05 \pm 3.42$ s

Figure 14. Same as Figure 13 but the minimization of eigenvalue technique is used, leading to a more linear particle motion pattern (Liu *et al.*, 2008).
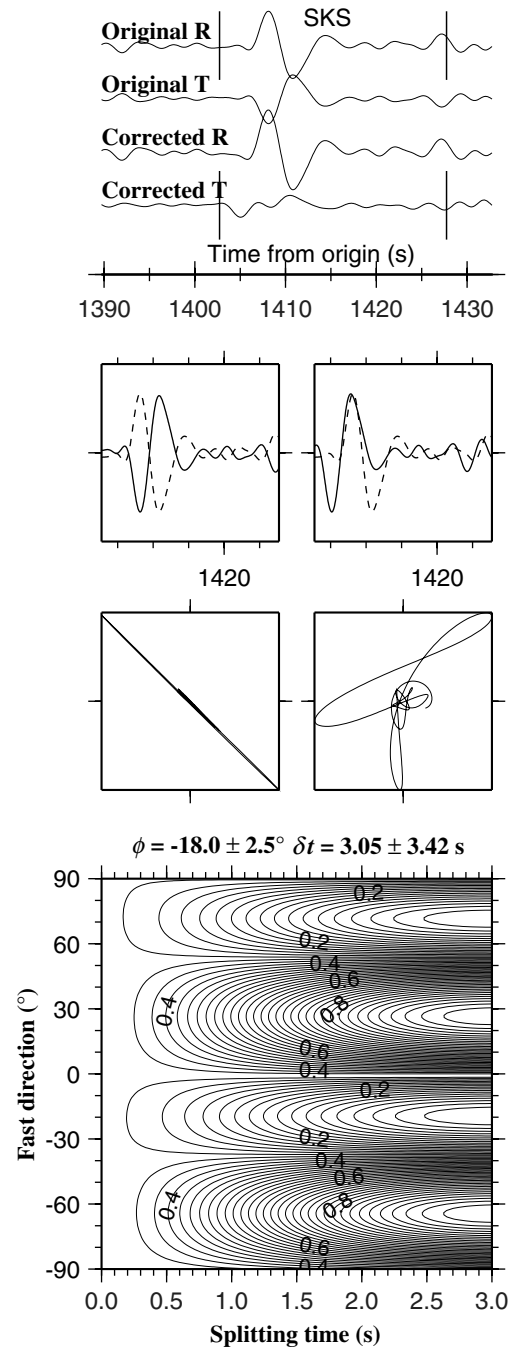
Figure 15. An event recorded by a station in the New Madrid Seismic Zone. Note the perfect linearity in the original particle motion pattern resulted from a malfunctioning horizontal component.

common causes of this problem. The results of the malfunctioning cannot be easily seen on the original radial and transverse components, which are created by rotating the north–south and east–west components according to the back azimuth of the event. The most important diagnostic for this problem is the perfectly linear pattern on the original particle motion diagram (Fig. 15). The corrected particle motion pattern is usually not linear, and the energy on the transverse component cannot be effectively removed.

Another form of instrumental malfunctioning is numerous spikes on one or both of the horizontal components. These spikes usually have the simple form of a one-sided Gaussian function and occur repeatedly. The resulting fast and slow components from these spikes rarely match with each other, and consequently, the corrected particle motion pattern is far from linear.

Dismissal of Good Measurements

Most of the Quality C measurements were ranked by the automatic procedure, and the rest were given by the operator during the manual screening stage. The final step of the manual screening is to make sure that most or all the acceptable measurements are included in the SWS database. One of the effective ways is to visually inspect all the Quality C measurements and verify the waveforms for station–event pairs with small (e.g., ≤2.5 s for most areas) splitting times and also small (e.g., ≤0.5 s) SDs for splitting times.

As discussed above, no matter whether the anisotropy is simple or complex, a common feature is that events with nearby ray-piercing points (or events from approximately the same source region) should have similar splitting parameters. While this is physically reasonable and should be considered as a criterion for the quality of a data set, one must be very careful when dismissing "outliers" that are measurements inconsistent with the rest of the events with nearby piercing points. Such outliers should be examined carefully. If they are truly reliable measurements, they should be kept in the SWS data set. They may contain valuable information about the particular earthquake or the structure of the part of the Earth's interior traveled by the *XKS* rays.

Conclusions

In spite of the apparent simplicity in performing SWS measurements, producing reliable SWS measurements requires a wide spectrum of seismological knowledge and skills, including seismic wave propagation, noise characterization, principle and operation of modern seismographs, and digital signal analysis and processing. Additionally, experience obtained in performing numerous splitting measurements is necessary in order to avoid mistakes caused by noise of various types, non-*XKS* seismic arrivals, and instrumental problems. A great deal of effort is required to adjust the *XKS* window, modify filtering parameters if necessary, and verify and change the quality ranking given by the automatic procedure. A highly reliable SWS data set cannot be obtained without such effort.

Data and Resources

All the seismic data used in the study were obtained from the IRIS DMC (http://www.iris.edu/data/; last accessed December 2012). The data set is publicly accessible.

References

Alsina, D., and R. Snieder (1995). Small-scale sublithospheric continental mantle deformation: Constraints from *SKS* splitting observations, *Geophys. J. Int.* **123,** 431–448.

Ando, M. (1984). ScS polarization anisotropy around Pacific Ocean, *J. Phys. Earth* **32,** 179–195.

Ekstrom, G., and R. W. Busby (2008). Measurements of seismometer orientation at USArray Transportable Array and backbone stations, *Seismol. Res. Lett.* **79,** 554–561, doi: 10.1785/gssrl.79.4.554.

Gao, S. S., and K. H. Liu (2009). Significant seismic anisotropy beneath the southern Lhasa Terrane, Tibetan Plateau, *Geochem. Geophys. Geosys.* **10,** Q02008, doi: 10.1029/2008GC002227.

Gao, S. S., K. H. Liu, and M. G. Abdelsalam (2010). Seismic anisotropy beneath the Afar depression and adjacent areas: Implications for mantle flow, *J. Geophys. Res.* **115,** B12330, doi: 10.1029/2009JB007141.

Gao, S. S., P. M. Davis, H. Liu, P. D. Slack, Y. A. Zorin, V. V. Mordvinova, V. M. Kozhevnikov, and R. P. Meyer (1994). Seismic anisotropy and mantle flow beneath the Baikal rift zone, *Nature* **371,** 149–151.

Levin, V., D. B. Okaya, and J. C. Park (2007). Shear wave birefringence in wedge-shaped anisotropic regions, *Geophy. J. Int.* **168,** 275–286.

Liu, K. H. (2009). NA-SWS-1.1: A uniform database of teleseismic shear-wave splitting measurements for North America, *Geochem. Geophys. Geosystems* **10,** Q05011, doi: 10.1029/2009GC002440.

Liu, K. H., and S. S. Gao (2011). Estimation of the depth of anisotropy using spatial coherency of shear-wave splitting parameters, *Bull. Seismol. Soc. Am.* **101,** no. 5, 2153–2161, doi: 10.1785/0120100258.

Liu, K. H., S. S. Gao, Y. Gao, and J. Wu (2008). Shear-wave splitting and mantle flow associated with the deflected Pacific slab beneath northeast Asia, *J. Geophys. Res.* **113,** B01305, doi: 10.1029/2007JB005178.

Long, M. D., and P. G. Silver (2009). Shear wave splitting anisotropy: Measurements, interpretation, and new directions, *Surv. Geophys.* 407–461.

Menke, W., and V. Levin (2003). The cross-convolution method for interpreting *SKS* splitting observations, with application to one and two-layer anisotropic earth models, *Geophys. J. Int.* **154,** 379–392.

Refayee, H. A., B. B. Yang, K. H. Liu, and S. S. Gao (2013). Mantle flow and lithosphere-asthenosphere coupling beneath the southwestern edge of the North American Craton: Constraints from shear-wave splitting measurements, *Earth Planet. Sci. Lett.* doi: 10.1016/j.epsl.2013.01.031.

Savage, M. K. (1999). Seismic anisotropy and mantle deformation: What have we learned from shear wave splitting? *Rev. Geophys.* **37,** 65–106.

Savage, M. K., and P. G. Silver (1993). Mantle deformation and tectonics: Constraints from seismic anisotropy in western United States, *Phys. Earth Planet. In.* **78,** 207–227.

Silver, P. G. (1996). Seismic anisotropy beneath the continents: Probing the depths of geology, *Annu. Rev. Earth Planet. Sci.* **24,** 385–432.

Silver, P. G., and W. W. Chan (1991). Shear wave splitting and subcontinental mantle deformation, *J. Geophys. Res.* **96,** 16,429–16,454.

Silver, P. G., and M. Savage (1994). The interpretation of shear wave splitting parameters in the presence of two anisotropic layers, *Geophys. J. Int.* **119,** 949–963, doi: 10.1111/j.1365-246X.1994.tb04027.x.

Teanby, N. A., J.-M. Kendall, and M. van der Baan (2004). Automation of shear-wave splitting measurements using cluster analysis, *Bull. Seismol. Soc. Am.* **94,** 453–463.

Tian, X., J. Zhang, S. Si, J. Wang, Y. Chen, and Z. Zhang (2011). *SKS* splitting measurements with horizontal component misalignment,

Geophys. J. Int. **185,** 329–340, doi: 10.1111/j.1365-246X.2011 .04936.x.

Vecsey, L., J. Plomerova, and V. Babuska (2008). Shear-wave splitting measurements: Problems and solutions, *Tectonophysics* **426,** 178–196.

Vinnik, L. P., V. Farra, and B. Romanowicz (1989). Azimuthal anisotropy in the Earth from observations of *SKS* at GEOSCOPE and NARS broadband stations, *Bull. Seismol. Soc. Am.* **79,** 1542–1558.

Wustefeld, A., and G. Bokelmann (2007). Null detection in shear-wave splitting measurements, *Bull. Seismol. Soc. Am.* **97,** 1204–1211, doi: 10.1785/0120060190.

Wustefeld, A., G. Bokelmann, C. Zaroli, and G. Barruol (2008). SplitLab: A shear-wave splitting environment in Matlab, *Comput. Geosci.* **34,** 515–528, doi: 10.1016/j.cageo.2007.08.002.

Department of Geological Sciences and Engineering
Missouri University of Science and Technology
Rolla, Missouri 65409
liukh@mst.edu
sgao@mst.edu